Supplementary Material

Altered Cross-frequency Coupling in Resting-State MEG after Mild Traumatic Brain Injury

Marios Antonakakis[1], Stavros I. Dimitriadis[2,3] , Michalis Zervakis[1], Sifis Micheloyannis[4] , Roozbeh Rezaie[5,6], Abbas Babajani-Feremi[5,6], George Zouridakis[7,8,*] and Andrew C. Papanicolaou[5,6,9]

[1] Technical University of Crete, Department of Electronic and Computer Engineering, Greece

[2]Artificial Intelligence and Information Analysis Laboratory, Department of Informatics, Aristotle University, Thessaloniki, 54124, Greece

[3]NeuroInformatics.GRoup, Aristotle University of Thessaloniki, Greece

[4] School of Medicine, University of Crete, Greece

[5]Department of Pediatrics, Division of Clinical Neurosciences, University of Tennessee Health Science Center, Memphis, TN, USA

[6]Neuroscience Institute, Le Bonheur Children's Hospital, Memphis, TN, USA

[7]Basque Center on Cognition, Brain and Language (BCBL), Paseo Mikeletegi 69, 20009 Donostia-San Sebastián, Spain

[8]Biomedical Imaging Lab, Departments of Engineering Technology, Computer Science, Biomedical Engineering, and Electrical and Computer Engineering, University of Houston, Houston, TX 77204, USA

[9]Department of Neurobiology and Anatomy, University of Tennessee Health Science Center, Memphis, TN, USA

[10]Corresponding author, phone: +30 28210 37206, Fax: +30 28210, 37542, email: mantonakakis@isc.tuc.gr, antonakakismar@gmail.com (Antonakakis Marios).

[*] GZ was Visiting Professor at BCBL under an Ikerbasque Fellowship during the development of this study. His permanent appointment is with the University of Houston.

1. A data-driven thresholding scheme

The example of Figure S.1**Error! Reference source not found.** illustrates how the edges, the GCE, and the GE functions change when the threshold for the cost of a graph changes for a control subject in the δ-β frequency range. Following this global network cost filtering that was used to identify significant links, we applied a data-driven thresholding scheme based on maximization of global cost-efficiency as a function of network cost.

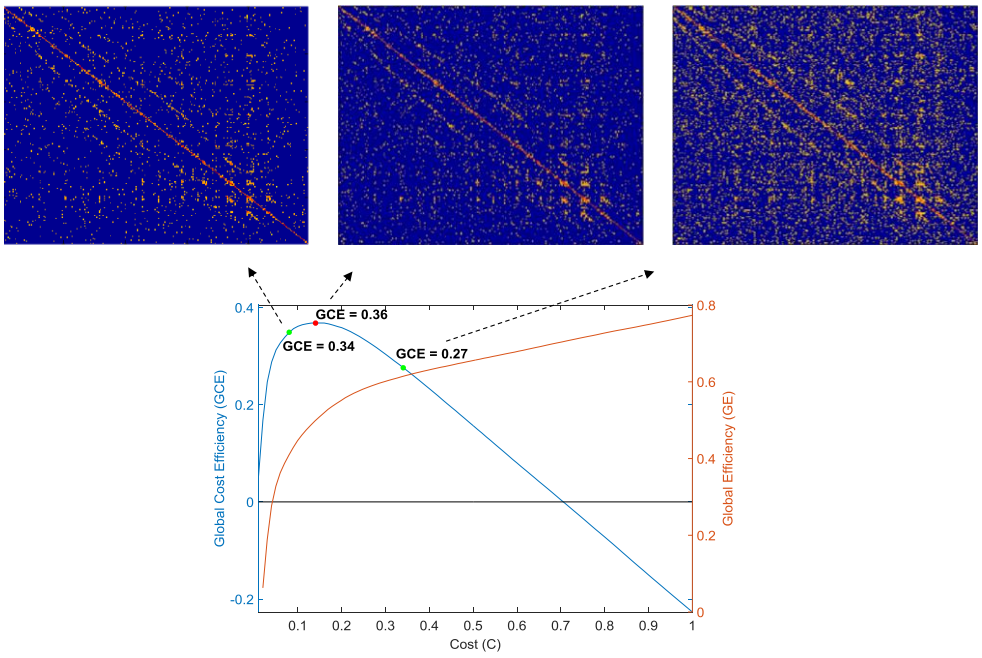

Figure S.1. Global cost efficiency as a function of network cost. Three examples of graphs with significant links for the δ-β frequency pair from a control subject. The red dot corresponds to the maximum value (optimal threshold) of global cost efficiency while the green dots represent non-optimal thresholds.

2. Feature Extraction and Classification

TSA learning of FCG patterns

- **Linear Dimensionality Reduction in Tensor Space**

The generic problem of linear dimensionality reduction in the second order space is the following. Given a set of tensors (i.e. matrices) $X_1, \ldots, X_m \in R^{n_1} \otimes R^{n_2}$ (where X be a $n_1 \times n_2$ FCG) find two transformation matrices U of size $n_1 \times k_1$ and V of $n_2 \times k_2$ that maps these mm tensors to a set of tensors $Y_1, \ldots, Y_m \in R^{k_1} \otimes R^{n_2}$, such that Y_i "represents" X_i, where $Y_i = U^T X_i V$. The method is of

particular interest in the special case where $\mathrm{X}_1, \ldots, \mathrm{X}_\mathrm{m} \in \mathrm{M}$ and M is a nonlinear sub-manifold embedded in $\mathrm{R}^{\mathrm{n}_1} \otimes \mathrm{R}^{\mathrm{n}_2}$.

- **Optimal Linear Embedding**

The ''true'' domain of FCGs most probably forms a nonlinear sub-manifold embedded in the ambient space of 2nd order tensors. Current approach using the TSA attempts to find a linear subspace approximation to the sub-manifold in the sense of local isometry. The adopted technique is the *tensorial* counterpart of *Locality Preserving Projection* (LPP).

Given a set of m tensors $X_{i=1:m}$, with each one being the tabular version of a single-trial FCG and having associated the cognitive load level as class label,, TSA starts by building an $\mathrm{m} \times \mathrm{m}$ weight-matrix S that represents the nearest neighbour graph G among the tensors. In our implementation, the element S_{ij} was set as

$$S_{ij} = \begin{cases} \exp\left(-\frac{\|X_i - X_j\|^2}{t}\right) & \text{condition}^1 \\ 0 & \text{otherwise} \end{cases} \quad (4)$$

where t is a control-parameter usually referred as ''radius of influence'' and condition^1 states that $\mathrm{X}_\mathrm{i}, \mathrm{X}_\mathrm{j}$ should share the same class label and anyone of them is among the kk-nearest neighbors of the other; the functional in (4) is known as heat kernel (here is employed with frobenius norm).

Then TSA seeks two transformation matrices U and V, such that when applied to each tensor to result in a mapping that would preserve the neighborhood relations encoded in G. Mathematically is formulated in the form of the below objective function:

$$\min_{U,V} \sum_{ij} \|U^T X_i V - U^T X_j V\|^2 S_{ij} \quad (5)$$

that incurs a heavy penalty if neighboring tensors and of the same class are mapped far apart. By denoting with D the diagonal matrix with elements $\mathrm{D}_{\mathrm{ij}} =$, the above optimization problem is reformulated as two coupled problems of eigenvector analysis:

$$(D_U - S_U)\mathrm{v} = \lambda D_U \mathrm{v} \quad (6)$$

$$D_U = \sum\nolimits_i D_{ii} X_i^T U U^T X_i \,, S_U = \sum\nolimits_{ij} S_{ij} X_i^T U U^T X_j$$

$$(D_V - S_V)\mathrm{u} = \lambda \mathrm{D_v u} \quad (7)$$

$$D_V = \sum\nolimits_i D_{ii} X_i V V^T X_i^T \,, S_V = \sum\nolimits_{ij} S_{ij} X_i V V^T X_j^T$$

The optimal U and V can be obtained by iteratively computing the generalized eigenvectors of (6) and (7) (after initializing U with the identity matrix).

In the present study, the dimensionality of the reduced tensors (i.e. the numbers of eigenvectors for the mapping $Y_i = U^T X_i V$) was optimized, via cross-validation, for each subject independently so as to achieve the highest classification performance. The numbers of neighbors and the heat parameter were set in a similar way.

3. Learning machines for classification

Ensemble learning is an effective technique that has increasingly been adopted to combine multiple learning algorithms to improve overall prediction accuracy (Dietterich et al., 2000). Subspace ensembles also have the advantage of using less memory than ensembles with all predictors, and can handle missing values. The random subspace ensemble classifiers perform relatively inferior to other ensemble classifiers (Ho, 1998; Bertoni et al., 2005; Kuncheva et al., 2010). *Random subspace* method has been used for linear classifiers as nearest neighbor (Skurichina, 2002). These group of ensemble methods are particularly useful for high-dimensional datasets (as in our case) because increased classification accuracy can be achieved by generating multiple prediction models each with a different feature subset (Bertoni et al., 2005; Kuncheva et al., 2010). Using an implantation delivered by ensemble classification toolbox of MATLAB (The MathWorks, Inc., Natick, MA, USA), the ensemble classification of the random space method evaluated using with 5 predictors per learner (the lowest cross-validated error) and totally 20 learners in the ensemble which was the smallest number that gave high classification performance.

ELM is as an emerging learning technique provides efficient unified solutions to generalized feed-forward networks including but not limited to (both single- and multi-hidden-layer) neural networks. ELM theory (Huang et al., 2006) showed that hidden neurons are important but can be randomly generated and independent from applications, and that ELMs have both universal approximation and classification capabilities. ELM selected in the classification scheme due to its computational elegancy and fast-learning capabilities, which lead to competitive performance with respect to other contemporary learning algorithms like back propagation neural networks (BPNNs), radial basis function networks (RBFNs) and support vector machines (SVMs) (Kim et al., 2009).

4. Consensus community detection in brain networks

Most of the currently available community-detection methods are not deterministic and their results typically depend on initial random seeds, initial conditions, and tie-break rules adopted for their

operation. An example of a non-deterministic algorithm is the adopted Louvain method (Blondel et al., 2008). Consensus clustering is usually employed in network analysis to generate stable results out of partitions generated by a high number of runs of the same stochastic method (Lancichinetti and Fortunato, 2012). The following highlight the algorithmic steps applied in order to identify stable clusterings across the groups.

1) Apply the Louvain method on each group-averaged FCG graph (Bassett et al., 2006).
2) Compute the group consensus matrix D, where D_{ij} is the number of partitions in which vertices i and j of the FCG graph are assigned to the same cluster across iterations and subjects S, divided by S.
3) Repeat steps 1 and 2.
4) Estimate the distance of the D matrix between 1st and 2nd iterations based on the variation of information (VI)[1] metric (Meila, 2007; Dimitriadis et al., 2009,2012a,b). A value of 0 denotes similar partitions, while higher values of VI indicate that the distance between the clusters has increased.
5) If the VI value at iteration t is less than 0.005, then stop and present the clustering of group consensus matrix D. Otherwise, go back to Step 1 for the next iteration.

Figure S2 illustrates how the variation of information metric, VI, between consecutive iterations of the algorithmic procedure converges to a stable partition, while Fig. S3 presents prototype clusterings for both groups in the five frequency pairs. The five most significant clusterings in the group of normal controls for the frequency pairs (δ-β), (δ-γ1), and (θ-β) were spatially restricted while in mTBI patients they were more distributed (Fig. S3 a-c). In frequency pairs (θ-γ1) and (β-γ2), the clusterings were spatially scattered in both groups. Furthermore, the organization of functional clusters differed in both groups across the five frequency pairs (Fig. S3 d, e).

5. Physical distance of sensors versus PAC strength

To uncover how the strength of CFC was distributed over the Euclidean distance between the sensors in the five frequency pairs across the two groups, we adopted a heat map representation of CFC with physical distance of sensors (Kolchinsky et al., 2014). This approach gave a clear view of how PAC strength was affected by Euclidean distance in both groups for each CFC-pair. Both Euclidean distance and CFC strength were equally divided into 50 bins.

[1] http://users.auth.gr/~stdimitr/software.html

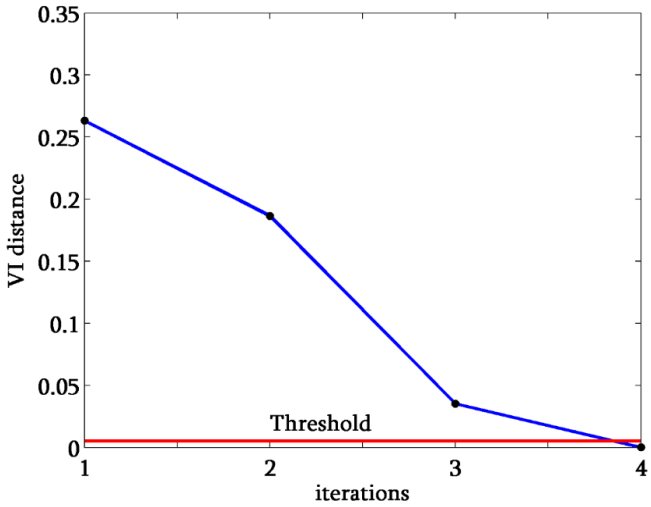

Figure S2. VI values between consecutive iterations of the algorithm used to detect stable clusterings across the two group. The red horizontal line corresponds to a threshold of 0.005 for the difference between the VI iteration t+1 and t.

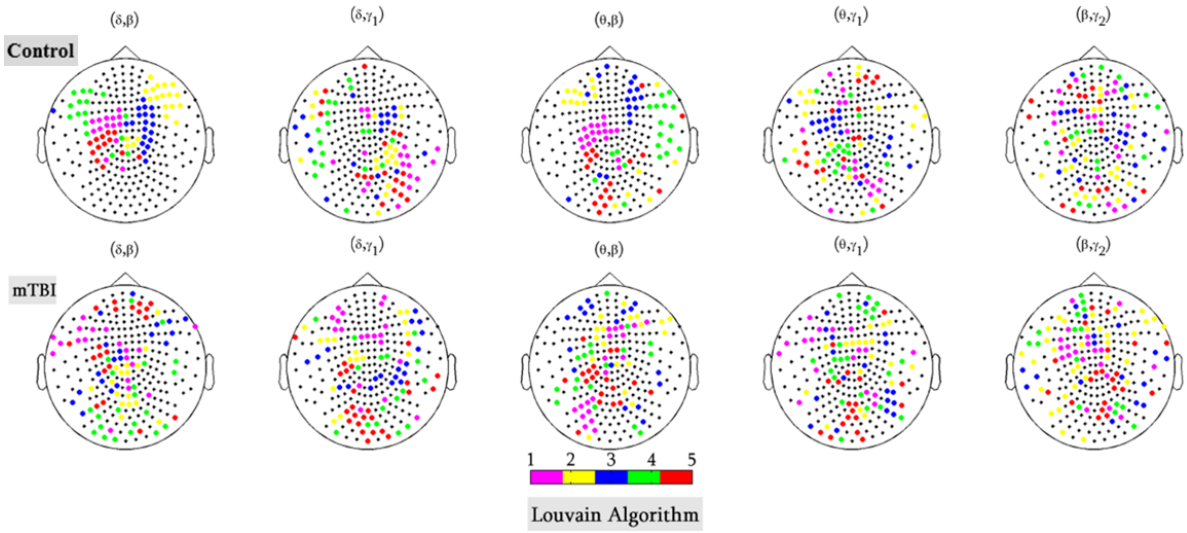

Figure S3. The five prototypical functional segmentations of FCGs with the highest average within-group strength are illustrated for each of the five frequency pairs in the two groups.

The mean CFC strength was distributed almost equally along the physical distance of sensors in both groups at frequency pairs δ-β (Fig.S4.a), δ-γ1 (Fig.S4.b) and θ-β (Fig.S4.c) but the group of normal controls showed higher values for the most range of physical distance. For the remaining two frequency pairs, θ-γ_1 (Fig.S4.d) and β-γ_2 (Fig.S4.e), the mean strength in the control group was marginally higher compared to mTBI patients, while mTBI subjects showed a few strong and distant connections on the tail of the distributions.

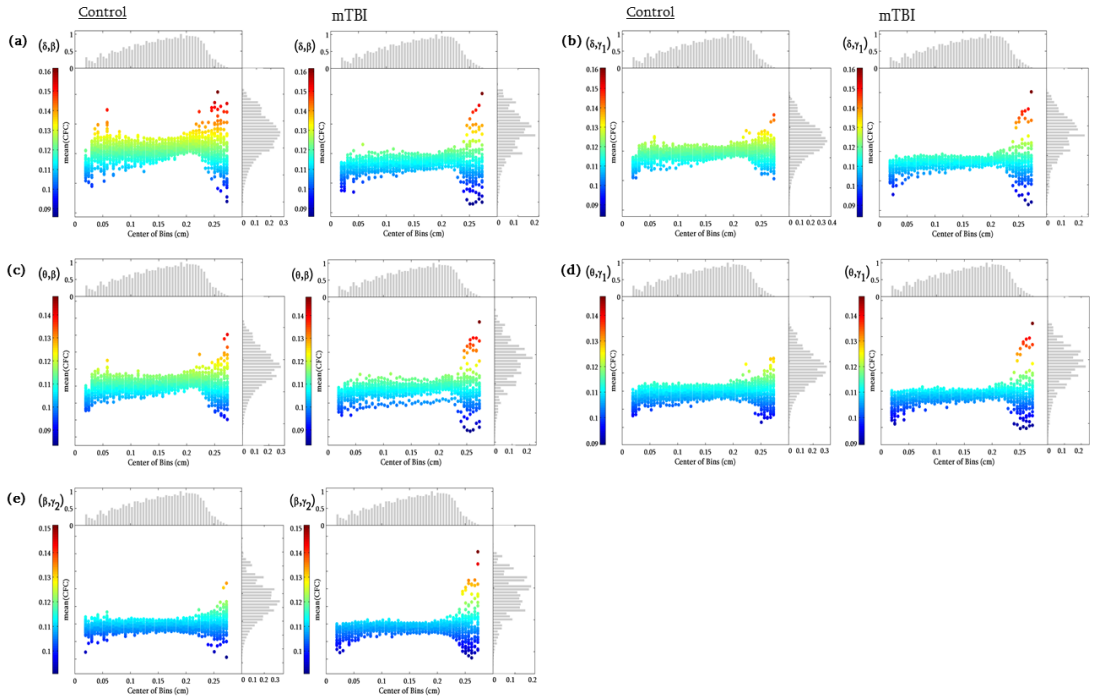

Figure S4. Heat maps (number of subjects x 50 bins) for various frequency pairs. The histogram on the top of each map presents the physical distance among the MEG sensors and the histogram on the right of each map represents the connectivity distances.

6. Relative Power

We calculated relative power (RP) to analyze the spectral content of MEG recordings. This measure represents the relative contribution of several oscillatory components to the global power spectrum. In comparison with absolute power, RP provides independent thresholds from the recording equipment and lower inter-subject variability (Leuchter *et al* 1993, Rodriguez *et al.* 1999).

We computed RP at every sensor in the conventional frequency bands: δ band (1–4 Hz), RP(δ); θ band (4–8 Hz), RP(ϑ); α band (8–15 Hz), RP(α); β band (15–30 Hz), and γ band (30–60 Hz), RP(γ). Group differences were estimated with Wilcoxon Rank-sum test in every frequency band ($p < 0.0001$, Bonferroni corrected – $p' < p/248$). Topographies of group-averaged RP are shown in Figure S.5, where the white circles denote the significantly different RPs.

The main findings are the higher RP for normal subjects compared to mTBI in the δ frequency band over bilateral frontal brain areas, while the opposite effect was observed in frequency bands θ to β for mTBI subjects, which demonstrated higher RP over bilateral frontal areas compared to normal controls.

Adopting Laplacian score (LS) as a feature extraction algorithm (Laskaris et al., 2013) and a cross-validation scheme as it is described in the following sections, we attempted to estimate the classification

of two groups based on RPs. At every fold of the 5-fold cross-validation, we re-estimated the LS_{Fr_S} of each of the 5 x 248 RPs — frequency bands (Fr) x sensors (S) — and employed a bootstrapping technique by randomizing the labels assigned to each feature for 100.000 times. At each run, a LS_{Fr_S} was estimated for each of the 5 x 248 RPs which finally ended to a null distribution of $LS^R_{Fr_S}$obtained for every feature (5 x 248 RPs). Next, it was tested whether each the $LS_{Fr_S}$of each feature deviated from the random and a (one-sided) p-value was assigned as the percentage of $LS^R_{Fr_S}$ that exceeded the original estimated LS_{Fr_S}. Then, the obtained p-values were Bonferroni-corrected for multiple comparisons (p' < 0.05/(5*248)). Finally, we adopted a k-nearest neighbor (k-NN) classifier using the majority vote criterion. For comparison purposes, we also employed a linear SVM classifier. Table S2 summarizes the classification performance, the specificity, sensitivity, number of features employed, and their distribution over frequency bands.

Table S2. Classification performance (averaged across 5 – folds of cross-validation) with k-NN and linear SVMs classifiers.

kNN			Linear SVMs			
Accuracy (%)	Sensitivity (%)	Specificity (%)	Accuracy (%)	Sensitivity (%)	Specificity (%)	Number of features δ-θ-α-β-γ
68.14 ± 9.14	65.87 ± 5.27	64.75 ± 10.12	71.56 ± 9.67	67.86 ± 9.805	66.94 ± 10.85	7-4-0-0-0

Finally, the classification scheme that included the feature extraction algorithm revealed significant differences in RP in the δ and θ frequency band mainly in frontal brain areas (Figure S.2). The findings related to the δ frequency band could be attributed possibly to the deactivation of the default mode network (DMN) resulting from inhibitory mechanisms activated during mental tasks (Dimitriadis et al., 2010). This finding may also reflect a less 'standby' DMN network for mTBI that otherwise would be ready to be activated during a cognitive task. The higher RPs for mTBI subjects in the θ frequency band over frontal areas could be interpreted as a compensatory mechanism to lower RP in the δ band for keeping the reflexibility of the cognitive state during spontaneous activity on a 'quasi-normal' level (Scheeringa et al., 2008) (S.1).

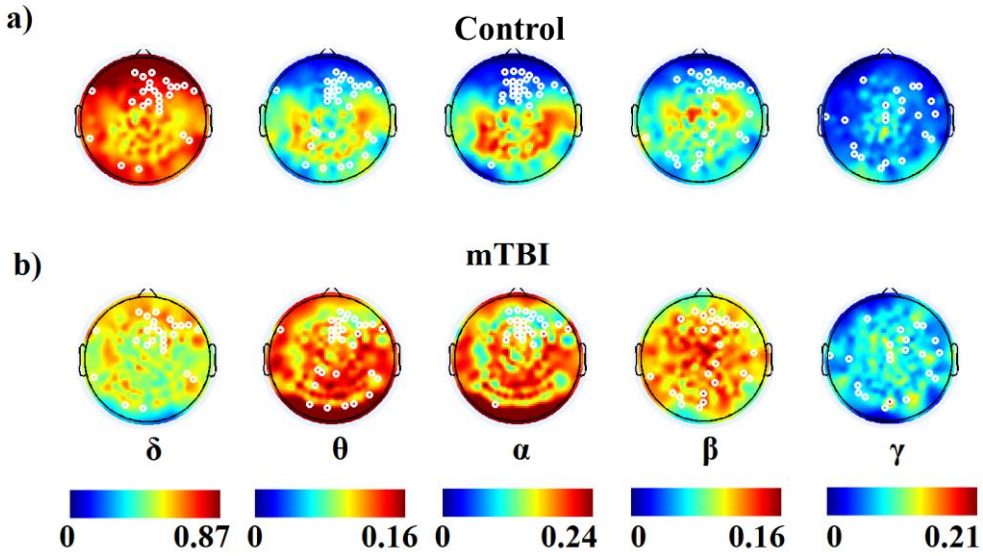

Figure S.5. Topography of the mean RP for each frequency band and group. White circles denote the statistically significant group difference of RP at the sensor level, using the Wilcoxon Rank-sum test ($p < 0.0001$, Bonferroni corrected – $p' < p/248$).

7. Vectorization Approach as classification scheme

a. Classification Scheme on the raw values

Apart from the proposed scheme in the main text, which denoted as ''TSA + k-NN or ENS or ELM'', we also employed a classification scheme on the raw CFC FCGs and their GE and LE values. In addition, in order to do a complete comparison, we also follow a classification scheme without the use of feature selection algorithm and a more conventional classification scheme denoted as ''LDA + k-NN or ENS or ELM'' against on the raw FCGs and their GE/LE values. In the latter, the FCG-related tensors were first vectorized (i.e., represented as high dimensional vectors by traversing the corresponding matrices in a systematic way), then dimensionality was reduced via LDA (linear discriminant analysis) () and classification was performed via standard k-NN/ENS/ELM algorithm for the comparison of performance with the main classification approach (TSA+knn/elm/ens), using as input control (50x248x248) and mTBI (30x248x248) vectors. In order to provide a statistical comparison between the two dimensionality reduction methods, we performed a statistical analysis within the 10-fold values (Table S3). Therefore the grey-washed colored cells represent the statistical significant difference, for instance, between the accuracies of TSA and LDA for the frequency pair δ,β. The results of these approaches are presented in Table S3 and S4. Finally, following same classification scheme as the case of the raw GE/LE, Table S5 illustrates the classification results for the GE/LE values of the thresholded FCGs.

Table S3: Classification performance (averaged across 10 – folds of cross-validation) with k-NN, ENS and ELM of the raw FCGs i) without feature selection algorithm ii) using TSA iii) using LDA. The grey-washed colored cells reveal the statistical difference between the corresponding performances for the two reduction dimensionality methods.

Classification of CFC FCGs									
	without feature selection (vectorized FCGs)			with TSA (original matrix format of FCG)			with LDA (vectorized FCGs)		
kNN									
frequency couple	Accuracy (%)	Sensitivity (%)	Specificity (%)	Accuracy (%)	Sensitivity (%)	Specificity (%)	Accuracy (%)	Sensitivity (%)	Specificity (%)
(δ,θ)	100±0	100±0	100±0	100±0	100±0	100±0	100±0	100±0	100±0
(δ,α)	100±0	100±0	100±0	100±0	100±0	100±0	99.58±0.7217	100±0	99.17±1.443
(δ,β)	100±0	100±0	100±0	100±0	100±0	100±0	91.67±7.217	100±0	83.33±14.43
(δ,γ1)	100±0	100±0	100±0	98.67±1.394	97.33±2.789	100±0	85.83±11.27	100±0	75.67±17.79
(δ,γ2)	57.5±0	32±7.204e-15	100±0	74±1.491	48.67±3.801	99.33±1.491	52.08±3.608	55±3.333	44.05±2.062
(θ,α)	48.75±0	18±5.695e-15	100±0	82.33±0.9129	64.67±1.826	100±0	62.5±12.5	83.33±6.41e-15	50.95±8.611
(θ,β)	50±0	20±4.271e-15	100±0	90.67±0.9129	84±1.491	97.33±1.491	91.25±6.495	89.17±5	82.83±12.71
(θ,γ1)	48.81±0.2795	18.1±0.4472	100±0	87.67±2.528	75.33±5.055	100±0	70.83±10.63	82.5±5	58.74±8.856
(θ,γ2)	50±0	20±3.925e-15	100±0	78.67±1.394	59.33±1.491	98±2.981	61.67±13.13	53.33±9.813	50.85±8.703
(α,β)	50±0	20±3.713e-15	100±0	67.67±1.9	35.33±3.801	100±0	67.5±11.92	58.33±4.303	56.32±11.67
(α,γ1)	49.88±0.3847	19.8±0.6156	100±0	74.67±1.826	49.33±3.651	100±0	68.33±8.036	51.67±3.333	55.62±7.281
(α,γ2)	50±0	20±3.713e-15	100±0	70.33±1.826	40.67±3.651	100±0	71.25±9.437	73.33±2.722	59.84±9.704
(β,γ1)	51.56±0.5553	22.5±0.8885	100±0	70±2.041	40±4.082	100±0	53.33±16.79	37.5±7.391	46.74±11.1
(β,γ2)	50±0	20±4.175e-15	100±0	75.33±1.826	50.67±3.651	100±0	66.67±3.819	70.83±7.391	56.06±4.26
(γ1,γ2)	50.63±0.6412	21±1.026	100±0	67.33±2.789	34.67±5.578	100±0	42.92±5.637	45.83±1.667	40.12±2.78
ENS									
frequency couple	Accuracy (%)	Sensitivity (%)	Specificity (%)	Accuracy (%)	Sensitivity (%)	Specificity (%)	Accuracy (%)	Sensitivity (%)	Specificity (%)
(δ,θ)	100±0	100±0	100±0	70.42±2.5	54.44±1.925	100±0	62.5±0	100±0	0±0
(δ,α)	100±0	100±0	100±0	89.17±1.667	75.56±3.849	100±0	62.5±0	100±0	0±0
(δ,β)	100±0	100±0	100±0	98.33±1.361	91.11±5.092	100±0	62.5±0	100±0	0±0
(δ,γ1)	100±0	100±0	100±0	86.67±1.361	71.11±5.092	100±0	62.5±0	100±0	0±0
(δ,γ2)	78.81±3.771	68.7±5.667	95.67±3.078	75±1.361	43.33±3.333	100±0	62.5±0	100±0	0±0
(θ,α)	80.56±1.181	69.1±1.997	99.67±1.026	78.33±1.16e-14	53.33±1.11e-14	100±0	45.83±14.43	33.33±57.74	66.67±57.74
(θ,β)	89.63±2.899	85.7±5.038	96.17±2.236	88.33±4.082	87.78±1.925	99.17±1.667	54.58±29.59	33.33±57.74	90±17.32
(θ,γ1)	87.88±4.017	82.7±6.594	96.5±2.752	82.08±3.696	64.44±5.092	100±0	47.08±16.6	33.33±57.74	70±51.96
(θ,γ2)	87.69±3.096	86.1±4.745	90.33±4.312	72.08±4.167	45.56±3.849	99.17±1.667	45.83±14.43	33.33±57.74	66.67±57.74
(α,β)	87.44±2.643	82.1±4.278	96.33±4.032	70.42±2.5	58.89±7.698	100±0	45.83±14.43	33.33±57.74	66.67±57.74
(α,γ1)	87.06±2.606	81.5±3.993	96.33±3.226	68.33±1.925	55.56±3.849	100±0	37.5±0	0±0	100±0
(α,γ2)	87.56±3.405	85±4.026	91.83±4.39	80.42±2.846	42.22±1.925	100±0	45.83±14.43	33.33±57.74	66.67±57.74
(β,γ1)	86.31±3.101	79.7±4.462	97.33±3.521	70±1.421e-14	43.33±0	100±0	37.5±0	0±0	100±0
(β,γ2)	88.63±3.267	86.6±4.773	92±4.38	72.08±0.8333	50±3.333	100±0	45.83±14.43	33.33±57.74	66.67±57.74
(γ1,γ2)	87.94±3.175	84.9±4.564	93±4.312	66.67±0	60±0	100±0	54.17±14.43	66.67±57.74	33.33±57.74
ELM									
frequency couple	Accuracy (%)	Sensitivity (%)	Specificity (%)	Accuracy (%)	Sensitivity (%)	Specificity (%)	Accuracy (%)	Sensitivity (%)	Specificity (%)
(δ,θ)	85.81±3.634	92.63±4.029	80.54±5.207	77.22±0.9623	54.44±1.925	100±0	37.5±0	62.5±0	100±0
(δ,α)	78.56±4.161	89.42±3.968	71.05±6.604	87.78±1.925	75.56±3.849	100±0	37.5±0	62.5±0	100±0
(δ,β)	66.88±4.841	78.8±5.961	57.8±5.974	95.56±2.546	91.11±5.092	100±0	37.5±0	62.5±0	100±0
(δ,γ1)	68.06±5.463	80.08±5.745	NaN±NaN	85.56±2.546	71.11±5.092	100±0	37.5±0	62.5±0	100±0
(δ,γ2)	56.31±6.545	68.89±6.647	44.11±8.716	71.67±1.667	43.33±3.333	100±0	37.5±0	62.5±0	74.87±2.358
(θ,α)	48.69±5.856	60.67±6.157	NaN±NaN	76.67±1.005e-14	53.33±1.11e-14	100±0	37.5±0	62.5±0	94.38±1.25
(θ,β)	56.69±3.81	NaN±NaN	NaN±NaN	93.89±0.9623	87.78±1.925	100±0	42.5±5	62.5±0	94±1.78
(θ,γ1)	53.25±5.247	NaN±NaN	NaN±NaN	82.22±2.546	64.44±5.092	100±0	57.5±0	62.5±0	77.38±2.097
(θ,γ2)	52.69±4.905	65.3±6.198	39.99±6.554	72.78±1.925	45.56±3.849	100±0	46.67±8.036	62.5±0	70.37±1.315
(α,β)	51.75±6.557	65.38±8.481	NaN±NaN	79.44±3.849	58.89±7.698	100±0	40±2.5	62.5±0	64.25±1.555
(α,γ1)	50.81±4.575	NaN±NaN	NaN±NaN	77.78±1.925	55.56±3.849	100±0	40.83±2.887	62.5±0	89.88±3.065
(α,γ2)	53.06±4.79	NaN±NaN	NaN±NaN	71.11±0.9623	42.22±1.925	100±0	41.67±5.204	62.5±0	77.17±3.342
(β,γ1)	50.94±2.977	NaN±NaN	NaN±NaN	71.67±0	43.33±0	100±0	38.33±1.443	62.5±0	68.75±2.179
(β,γ2)	51.88±4.224	NaN±NaN	38.38±5.251	75±1.667	50±3.333	100±0	37.5±0	62.5±0	72.25±0.866
(γ1,γ2)	48.5±5.203	60.76±5.85	NaN±NaN	80±1.421e-14	60±0	100±0	40.83±1.443	62.5±0	61.75±0.5

Table S4: Classification performance (averaged across 10 – folds of cross-validation) with k-NN, ENS and ELM of the raw GE/LE values i) without feature selection algorithm ii) using LDA.

	Classification of Global Efficiency					
	without feature selection			with LDA		
	kNN					
frequency couple	Accuracy (%)	Sensitivity (%)	Specificity (%)	Accuracy (%)	Sensitivity (%)	Specificity (%)
(δ,θ)	100±0	100±0	100±0	100±0	100±0	100±0
(δ,α)	100±0	100±0	100±0	100±0	100±0	100±0
(δ,β)	100±0	100±0	100±0	94.38±0.7217	92.5±1.915	97.5±1.667
(δ,γ1)	100±0	100±0	100±0	98.44±0.625	97.5±1	100±0
(δ,γ2)	88.75±0	92±0	83.33±6.41e-15	87.19±2.577	86±2.828	89.17±3.191
(θ,α)	95.31±0.625	92.5±1	100±0	64.69±1.573	54±2.828	82.5±3.191
(θ,β)	96.88±0.7217	95±1.155	100±0	87.5±1.021	85.5±2.517	90.83±1.667
(θ,γ1)	97.19±0.625	95.5±1	100±0	75±2.041	74.5±4.123	75.83±1.667
(θ,γ2)	93.44±0.625	93.5±1	93.33±0	83.44±2.577	83±3.464	84.17±1.667
(α,β)	96.56±1.197	94.5±1.915	100±0	75.94±4.13	70.5±5.26	85±5.774
(α,γ1)	95.63±0.7217	93±1.155	100±0	61.88±2.602	64±2.828	58.33±3.333
(α,γ2)	93.75±0	94±0	93.33±1.11e-14	83.13±2.165	84±2.309	81.67±4.303
(β,γ1)	96.25±0	94±1.282e-14	100±0	44.69±0.625	45±1.155	44.17±3.191
(β,γ2)	94.69±0.625	95.5±1	93.33±6.41e-15	83.13±4.39	90.5±4.435	70.83±6.31
(γ1,γ2)	95±0	96±1.282e-14	93.33±9.065e-15	67.5±1.021	69.5±3.416	64.17±4.194
	ENS					
frequency couple	Accuracy (%)	Sensitivity (%)	Specificity (%)	Accuracy (%)	Sensitivity (%)	Specificity (%)
(δ,θ)	100±0	100±0	100±0	100±0	100±0	100±0
(δ,α)	100±0	100±0	100±0	100±0	100±0	100±0
(δ,β)	100±0	100±0	100±0	95.94±1.573	95.5±2.517	96.67±0
(δ,γ1)	100±0	100±0	100±0	98.75±1.021	98±1.633	100±0
(δ,γ2)	85.31±1.197	85±1.155	85.83±1.667	88.75±1.768	86.5±3.416	92.5±4.194
(θ,α)	94.69±0.625	91.5±1	100±0	64.69±1.875	56±1.633	79.17±3.191
(θ,β)	96.25±0	94±1.282e-14	100±0	87.81±2.135	86±3.266	90.83±4.194
(θ,γ1)	95.63±0.7217	93±1.155	100±0	75.63±0.7217	73±2.582	80±4.714
(θ,γ2)	92.5±1.021	92±1.633	93.33±9.065e-15	84.38±4.621	84.5±6.191	84.17±9.179
(α,β)	95.63±0.7217	93±1.155	100±0	75.31±3.442	70±3.651	84.17±7.391
(α,γ1)	95.31±0.625	92.5±1	100±0	60.94±2.135	62.5±2.517	58.33±6.939
(α,γ2)	92.5±1.021	92±1.633	93.33±9.065e-15	87.19±2.135	90±2.828	82.5±1.667
(β,γ1)	95.63±0.7217	93±1.155	100±0	48.44±4.13	47.5±4.123	50±4.714
(β,γ2)	92.81±0.625	92.5±1	93.33±6.41e-15	83.44±0.625	89.5±2.517	73.33±4.714
(γ1,γ2)	92.5±0	92±0	93.33±0	64.69±2.135	65.5±3	63.33±7.201
	ELM					
frequency couple	Accuracy (%)	Sensitivity (%)	Specificity (%)	Accuracy (%)	Sensitivity (%)	Specificity (%)
(δ,θ)	99.38±0.7217	100±0	98.75±1.443	100±0	100±0	100±0
(δ,α)	97.81±2.135	99.58±0.8333	96.75±4.272	100±0	100±0	100±0
(δ,β)	82.81±1.573	95.12±0.875	74.9±2.513	86.88±9.437	100±0	77.75±13.23
(δ,γ1)	86.56±1.197	95.49±1.199	80±0.5932	95.31±7.099	100±0	92.82±10
(δ,γ2)	67.5±7.84	NaN±NaN	NaN±NaN	80±2.282	95.66±5.571	68.63±4.343
(θ,α)	60.63±3.608	77.62±7.198	50.09±2.537	70±6.693	92.08±7.832	58±6.481
(θ,β)	70.31±4.254	87.38±2.689	59.89±5.079	85.31±11.96	88.83±7.184	82.58±18.77
(θ,γ1)	62.5±5.401	78.79±6.619	52.36±6.529	63.75±21.91	NaN±NaN	55.52±18.26
(θ,γ2)	61.88±2.976	75.83±4.641	52.2±4.441	80.31±6.485	94.37±6.555	70.33±7.261
(α,β)	61.25±2.7	71.79±5.391	52.86±3.276	73.44±18.33	86.29±12.27	64.54±22.49
(α,γ1)	55±1.443	68.88±2.939	42.66±2.337	58.75±16.3	NaN±NaN	49.99±13.31
(α,γ2)	68.75±3.227	78.77±3.975	57±5.013	82.19±6.24	86.19±9.894	NaN±NaN
(β,γ1)	49.69±4.828	61.64±4.299	35±7.279	35.94±10.58	45.67±16.23	26.65±3.94
(β,γ2)	67.19±4.828	79.41±4.324	58.11±5.218	71.25±8.72	83.98±12.82	64.5±11.09
(γ1,γ2)	55.31±5.141	NaN±NaN	44.13±4.881	65.31±5.039	91.5±10.79	52.67±3.963

	Classification of Local Efficiency					
	without feature selection			with LDA		
	kNN					
frequency couple	Accuracy (%)	Sensitivity (%)	Specificity (%)	Accuracy (%)	Sensitivity (%)	Specificity (%)
(δ,θ)	100±0	100±0	100±0	100±0	100±0	100±0
(δ,α)	100±0	100±0	100±0	100±0	100±0	100±0
(δ,β)	100±0	100±0	100±0	97.5±2.041	96±3.266	100±0
(δ,γ1)	100±0	100±0	100±0	99.69±0.625	99.5±1	100±0
(δ,γ2)	88.75±0	92±1.282e-14	83.33±0	93.75±6.535	93±9.018	95±10
(θ,α)	95.94±0.625	93.5±1	100±0	65.94±16.97	57.5±26.3	80±16.56
(θ,β)	96.56±1.197	94.5±1.915	100±0	83.75±10.61	79±13.11	91.67±11.06
(θ,γ1)	97.5±1.768	96±2.828	100±0	67.5±8.354	73.5±12.37	57.5±20.97
(θ,γ2)	93.13±0.7217	93±1.155	93.33±1.11e-14	90.63±9.492	95±10	83.33±14.66
(α,β)	95.63±0.7217	93±1.155	100±0	85.94±8.377	83.5±17.92	90±8.165
(α,γ1)	96.25±1.021	94±1.633	100±0	63.44±11.47	53.5±24.35	80±13.05
(α,γ2)	93.75±0	94±1.282e-14	93.33±0	82.81±14.38	81±14.74	85.83±16.41
(β,γ1)	96.25±0	94±1.282e-14	100±0	54.38±8.75	40±10.71	78.33±15.52
(β,γ2)	93.13±0.7217	93±1.155	93.33±6.41e-15	79.69±12.47	83.5±5.972	73.33±28.15
(γ1,γ2)	93.75±0	94±1.282e-14	93.33±0	70±5.774	71.5±21.44	67.5±23.15
	ENS					
frequency couple	Accuracy (%)	Sensitivity (%)	Specificity (%)	Accuracy (%)	Sensitivity (%)	Specificity (%)
(δ,θ)	100±0	100±0	100±0	100±0	100±0	100±0
(δ,α)	100±0	100±0	100±0	100±0	100±0	100±0
(δ,β)	100±0	100±0	100±0	94.06±7.731	91.5±13.1	98.33±3.333
(δ,γ1)	100±0	100±0	100±0	98.75±1.768	98±2.828	100±0
(δ,γ2)	85.94±1.573	87±2	84.17±1.667	79.38±9.922	84±8.485	71.67±20.09
(θ,α)	95±0	92±1.282e-14	100±0	68.13±6.333	60±15.58	81.67±26.74
(θ,β)	96.25±0	94±1.282e-14	100±0	94.38±9.601	96.5±4.435	90.83±18.33
(θ,γ1)	95.63±0.7217	93±1.155	100±0	91.25±5.774	90.5±8.386	92.5±12.87
(θ,γ2)	92.81±1.197	92.5±1.915	93.33±0	89.69±4.375	91±9.309	87.5±13.98
(α,β)	95.31±0.625	92.5±1	100±0	82.5±12.46	82.5±15.86	82.5±10.32
(α,γ1)	95±0	92±0	100±0	56.56±15.36	55.5±14.36	58.33±22.69
(α,γ2)	92.19±1.197	91.5±1.915	93.33±6.41e-15	89.38±4.27	86.5±5.508	94.17±11.67
(β,γ1)	96.25±0	94±1.282e-14	100±0	54.38±11.79	59±13.22	46.67±35.28
(β,γ2)	93.44±0.625	93.5±1	93.33±6.41e-15	83.75±7.217	85.5±9.983	80.83±25.59
(γ1,γ2)	94.38±0.7217	95±1.155	93.33±9.065e-15	76.56±19.08	79±23.8	72.5±18.93
	ELM					
frequency couple	Accuracy (%)	Sensitivity (%)	Specificity (%)	Accuracy (%)	Sensitivity (%)	Specificity (%)
(δ,θ)	99.06±0.625	100±0	98.13±1.25	100±0	100±0	100±0
(δ,α)	97.5±1.021	100±0	95±2.041	100±0	100±0	100±0
(δ,β)	88.13±4.841	97.13±1.674	81.9±8.207	91.56±2.772	99.58±0.8333	86.45±5.051
(δ,γ1)	84.38±2.165	94.63±0.8753	79.03±4.942	94.69±1.875	100±0	90.13±3.945
(δ,γ2)	70.94±4.492	78.79±5.661	64.08±4.93	86.25±1.768	97.62±1.917	78.67±3.551
(θ,α)	54.06±4.828	69.43±8.964	41.05±4.666	64.06±1.197	NaN±NaN	53.63±0.6985
(θ,β)	71.88±2.394	NaN±NaN	64.63±5.558	80±2.7	NaN±NaN	69.52±3.889
(θ,γ1)	60±10.46	73.41±10.26	51.24±13.62	73.44±2.772	NaN±NaN	63.65±4.215
(θ,γ2)	68.13±2.394	79.3±4.191	57.96±4.087	85.63±2.602	94.42±2.234	81.23±3.284
(α,β)	66.25±1.021	82.56±2.303	NaN±NaN	73.75±2.7	NaN±NaN	61.15±4.439
(α,γ1)	54.69±2.135	68.43±1.883	39.92±4.943	63.44±1.197	79.07±5.525	54.4±1.306
(α,γ2)	69.38±9.27	77.36±9.023	64.53±9.368	84.69±3.287	92.5±2.884	78.96±5.784
(β,γ1)	52.81±4.002	66.69±5.354	38.58±3.152	45±2.5	NaN±NaN	35.05±2.427
(β,γ2)	65.31±5.807	NaN±NaN	57.13±9.92	84.38±3.307	89.36±2.817	NaN±NaN
(γ1,γ2)	56.56±4.719	69.69±2.082	43.06±7.349	66.56±1.875	NaN±NaN	58.38±2.83

Table S5: Classification performance (averaged across 10 – folds of cross-validation) with k-NN, ENS and ELM of the GE/LE values of the thresholded FCGs i) without feature selection algorithm ii) using LDA.

	Classification of Global Efficiency of Th CFC FCGs					
	without feature selection			with LDA		
	kNN					
frequency couple	Accuracy (%)	Sensitivity (%)	Specificity (%)	Accuracy (%)	Sensitivity (%)	Specificity (%)
(δ,θ)	70.94±3.125	58±4.32	92.5±3.191	60±7.706	76±10.2	33.33±23.88
(δ,α)	74.38±2.602	81.5±1.915	62.5±5.693	64.06±10.02	58.5±8.386	73.33±16.56
(δ,β)	77.5±1.021	93.5±1	50.83±1.667	75.31±15.66	78±19.25	70.83±38.62
(δ,γ1)	69.69±4.492	81.5±3.416	50±7.201	67.19±11.29	74.5±11.7	55±26.18
(δ,γ2)	74.38±2.394	77±3.464	70±2.722	78.75±13.35	88.5±8.386	62.5±25.73
(θ,α)	63.13±2.602	67±2.582	56.67±4.714	59.38±8.75	67±8.246	46.67±14.4
(θ,β)	69.38±1.25	98±0	21.67±3.333	72.19±18.33	82±9.381	55.83±33.26
(θ,γ1)	74.38±0.7217	97.5±1	35.83±1.667	64.38±12.18	73±27.2	50±13.61
(θ,γ2)	73.75±0	100±0	30±5.551e-15	76.88±18.94	89±10.13	56.67±35.38
(α,β)	60.31±2.135	67±3.464	49.17±1.667	63.75±23.12	72.5±25.74	49.17±27.54
(α,γ1)	73.44±1.875	86.5±3.416	51.67±1.925	67.81±18.88	77.5±20.09	51.67±32.26
(α,γ2)	75.63±0.7217	100±0	35±1.925	69.38±12.6	70.5±22.35	67.5±27.27
(β,γ1)	61.88±0.7217	60.5±1.915	64.17±4.194	57.81±21.61	62.5±26.45	50±31.15
(β,γ2)	72.81±1.573	58.5±2.517	96.67±1.282e-14	82.81±10.77	86±13.66	77.5±8.767
(γ1,γ2)	73.75±3.062	79±2.582	65±4.303	74.69±10.63	85±10.13	57.5±25
	ENS					
frequency couple	Accuracy (%)	Sensitivity (%)	Specificity (%)	Accuracy (%)	Sensitivity (%)	Specificity (%)
(δ,θ)	63.13±1.25	99.5±1	2.5±3.191	59.69±11.2	58.5±6.191	61.67±22.85
(δ,α)	68.13±2.165	100±0	15±5.774	78.75±6.455	81.5±16.11	74.17±10.67
(δ,β)	64.38±1.25	100±0	5±3.333	64.06±13.05	68±25.56	57.5±31.67
(δ,γ1)	64.69±1.875	100±0	5.833±5	74.69±4.607	80±3.651	65.83±16.86
(δ,γ2)	72.19±1.875	99.5±1	26.67±6.086	72.19±14.73	75.5±23.8	66.67±6.086
(θ,α)	62.5±0	100±0	0±0	60.63±12.77	76±8.165	35±33.61
(θ,β)	63.44±0.625	100±0	2.5±1.667	72.81±7.595	81±9.592	59.17±5.693
(θ,γ1)	64.38±2.394	100±0	5±6.383	63.75±6.292	79.5±9.574	37.5±15.72
(θ,γ2)	65.63±1.614	99.5±1	9.167±3.191	73.13±12.18	90±7.483	45±27.95
(α,β)	62.5±1.021	99.5±1	0.8333±1.667	66.88±3.307	68.5±7.724	64.17±11.01
(α,γ1)	67.5±2.282	99.5±1	14.17±5	74.06±6.95	72.5±9.983	76.67±15.87
(α,γ2)	65.94±1.875	100±0	9.167±5	77.19±15.52	93±10.13	50.83±36.04
(β,γ1)	63.75±1.021	99±1.155	5±1.925	64.69±13.2	72±12.33	52.5±34.03
(β,γ2)	94.06±1.573	99.5±1	85±3.333	96.25±3.68	96.5±7	95.83±5
(γ1,γ2)	70.94±1.573	100±0	22.5±4.194	72.5±11.73	67.5±14.46	80.83±17.29
	ELM					
frequency couple	Accuracy (%)	Sensitivity (%)	Specificity (%)	Accuracy (%)	Sensitivity (%)	Specificity (%)
(δ,θ)	57.81±8.252	67.17±8.517	NaN±NaN	63.44±11.92	70.17±8.623	NaN±NaN
(δ,α)	62.19±4.492	73.62±2.002	NaN±NaN	60.94±6.799	75.44±12.05	51.08±10.59
(δ,β)	60.94±4.607	70.98±3.78	46.61±3.102	78.13±10.48	83.83±8.578	73.63±13.3
(δ,γ1)	59.06±6.404	67.82±6.919	49.95±5.221	62.5±3.68	69.72±1.695	NaN±NaN
(δ,γ2)	61.56±4.828	70.2±7.447	53.09±4.912	66.25±10.05	76.02±15	53.33±17.99
(θ,α)	49.06±4.719	59.78±4.2	37.17±6.849	53.44±17.18	58.55±16.73	NaN±NaN
(θ,β)	61.25±3.68	71.96±3.977	50.54±4.287	78.44±5.625	80.17±10.71	NaN±NaN
(θ,γ1)	64.38±6.884	74.79±10.08	55.63±6.875	71.25±6.847	81.35±12.18	NaN±NaN
(θ,γ2)	59.69±4.375	69.62±4.524	50.24±5.266	70.31±23.59	81.39±22.95	NaN±NaN
(α,β)	55±3.953	66.44±4.386	41.33±3.279	70±7.84	NaN±NaN	61.82±15.07
(α,γ1)	55.31±6.24	68.58±7.571	40.53±7.588	64.06±17.89	74.51±16.76	51.75±27.32
(α,γ2)	66.56±6.485	78.87±5.037	52.5±9.608	64.06±8.562	72.05±11.16	NaN±NaN
(β,γ1)	54.38±3.886	64.39±2.732	41.46±6.629	65.94±13.48	75.97±16.73	54.25±20.7
(β,γ2)	76.56±1.573	87.83±2.513	68.36±2.654	81.56±4.934	99.38±1.25	68.5±6.843
(γ1,γ2)	65±4.787	75.97±3.631	NaN±NaN	74.38±15.16	76.74±16.23	NaN±NaN

	Classification of Local Efficiency of Th CFC FCGs					
	without feature selection			with LDA		
	kNN					
frequency couple	Accuracy (%)	Sensitivity (%)	Specificity (%)	Accuracy (%)	Sensitivity (%)	Specificity (%)
(δ,θ)	68.13±1.614	65.5±3.416	72.5±1.667	56.56±16.56	56±27.28	57.5±30.47
(δ,α)	84.69±1.197	80.5±1.915	91.67±3.333	77.5±11.23	71.5±14.64	87.5±15
(δ,β)	62.19±1.197	39.5±1.915	100±0	92.19±7.526	94±10.71	89.17±11.34
(δ,γ1)	41.25±2.282	6±3.651	100±0	70.63±14.77	67.5±16.28	75.83±26.58
(δ,γ2)	43.75±1.021	10±1.633	100±0	70.63±22.6	62±26.98	85±25.75
(θ,α)	62.5±3.536	84±4.32	26.67±2.722	53.44±9.263	57.5±6.403	46.67±29.19
(θ,β)	77.5±1.443	100±0	40±3.849	69.38±14.88	78.5±16.44	54.17±30.72
(θ,γ1)	76.56±1.197	91.5±1.915	51.67±1.925	80.94±12.8	87±13.11	70.83±25.15
(θ,γ2)	39.69±1.197	3.5±1.915	100±0	88.75±3.227	93±8.246	81.67±21.34
(α,β)	69.38±3.307	74±1.633	61.67±6.383	79.69±4.13	81.5±12.26	76.67±22.61
(α,γ1)	65.63±0.7217	100±0	8.333±1.925	85.31±8.802	88.5±9.292	80±33.67
(α,γ2)	40.63±0.7217	5±1.155	100±0	80±10.36	78±7.832	83.33±15.4
(β,γ1)	64.06±0.625	97±2	9.167±4.194	67.19±14.59	78.5±14.55	48.33±36.26
(β,γ2)	81.88±1.614	71±2.582	100±0	97.19±4.828	96±8	99.17±1.667
(γ1,γ2)	63.13±1.614	95±2	10±6.086	53.75±10.85	49±14.28	61.67±19.15
	ENS					
frequency couple	Accuracy (%)	Sensitivity (%)	Specificity (%)	Accuracy (%)	Sensitivity (%)	Specificity (%)
(δ,θ)	62.5±0	100±0	0±0	75.94±2.135	80.5±15.09	68.33±21.34
(δ,α)	69.69±2.954	98.5±1.915	21.67±6.939	84.69±7.864	87.5±9.292	80±8.165
(δ,β)	80±2.7	90.5±3.786	62.5±3.191	77.19±14.8	82.5±19.14	68.33±8.819
(δ,γ1)	68.44±0.625	100±0	15.83±1.667	83.13±6.884	88.5±9.574	74.17±17.72
(δ,γ2)	81.25±2.282	92.5±1.915	62.5±5	81.25±8.72	73±18.65	95±7.935
(θ,α)	62.5±0	100±0	0±0	58.75±17.71	58±20.2	60±27.76
(θ,β)	63.75±1.021	100±0	3.333±2.722	84.38±5.637	92±5.888	71.67±11.39
(θ,γ1)	64.38±0.7217	100±0	5±1.925	73.75±16.01	78.5±15.18	65.83±23.31
(θ,γ2)	79.06±1.197	94±1.282e-14	54.17±3.191	80.31±9.375	84±11.43	74.17±17.29
(α,β)	62.5±0	100±0	0±0	70.63±6.166	84.5±11.59	47.5±17.08
(α,γ1)	62.5±0	100±0	0±0	80±8.292	84.5±9.434	72.5±13.44
(α,γ2)	80±1.021	97.5±1	50.83±3.191	93.13±4.621	89.5±7.724	99.17±1.667
(β,γ1)	62.5±0	100±0	0±0	57.19±9.595	67±25.01	40.83±32.59
(β,γ2)	92.81±2.772	98.5±1.915	83.33±4.714	99.69±0.625	100±0	99.17±1.667
(γ1,γ2)	62.5±0	100±0	0±0	54.69±23.55	57.5±33.56	50±29.19
	ELM					
frequency couple	Accuracy (%)	Sensitivity (%)	Specificity (%)	Accuracy (%)	Sensitivity (%)	Specificity (%)
(δ,θ)	58.13±9.869	NaN±NaN	NaN±NaN	74.69±10.23	94.25±5.217	64.24±13.08
(δ,α)	66.88±2.165	76.58±3.549	57.01±4.445	82.81±12.84	86.79±14.75	NaN±NaN
(δ,β)	67.19±3.442	82.33±8.301	57.77±3.076	90.31±4.492	99.17±0.9623	83.13±8.816
(δ,γ1)	59.69±5.984	70.65±5.031	NaN±NaN	76.56±9.756	93.5±9.434	66.36±11.74
(δ,γ2)	68.44±4.828	82.75±2.481	58.04±7.399	79.69±9.375	99.58±0.8333	68.52±10.65
(θ,α)	52.19±3.733	61.1±5.269	40.64±2.625	53.13±10.43	NaN±NaN	41.35±11.23
(θ,β)	63.75±5.401	73.08±3.469	54.87±9.737	75.31±10.82	78.44±8.521	71.88±17.3
(θ,γ1)	60.94±7.386	73.21±9.377	49.17±11.07	73.44±9.649	79.62±8.208	67.96±16.71
(θ,γ2)	67.5±5.303	80.57±6.407	57.25±5.28	71.56±9.375	88.08±11.2	59.57±9.337
(α,β)	59.06±5.625	68.72±6.676	NaN±NaN	69.06±14.38	73.74±7.156	65.67±25.19
(α,γ1)	63.13±2.976	73.45±3.877	53.58±6.739	70.94±10.33	76.58±4.518	66.21±20.37
(α,γ2)	66.88±5.154	78.46±5.398	58.7±7.718	75±8.6	94.58±2.44	62.65±8.842
(β,γ1)	54.69±7.996	66.49±11.83	43.96±7.301	59.38±15.5	NaN±NaN	48.06±14.24
(β,γ2)	80±6.535	87.33±5.98	74.21±9.073	98.44±2.366	100±0	96.88±4.732
(γ1,γ2)	50±7.706	63.97±6.75	NaN±NaN	37.19±1.875	NaN±NaN	30.59±4.898

b. Laplacian Scores

A second vectorization approach as classification scheme was also used in order to compare its performance with our main classification approach (TSA+knn/elm/ens), using as input control (50x248x248) and mTBI (30x248x248) vectors and as a feature selection algorithm the Laplacian Scores, LS (described in the previous section). First, we ran the LS algorithm for 1000 times to get a distribution regarding the features in order to estimate a threshold about the selection of the significant LS features. The selected features are plotted in Fig S.6 for each frequency couple and each subject. After feature selection, we used the k-NN algorithm to calculate the classification metrics, i.e., accuracy, sensitivity, and specificity in order to quantify the discrimination between the two groups (Table S6). Finally, the same procedure (i.e., feature selection and classification) was performed using as input the efficiency of the full weighted graphs. The results of this approach are presented in Table S7 and Figure S.7.

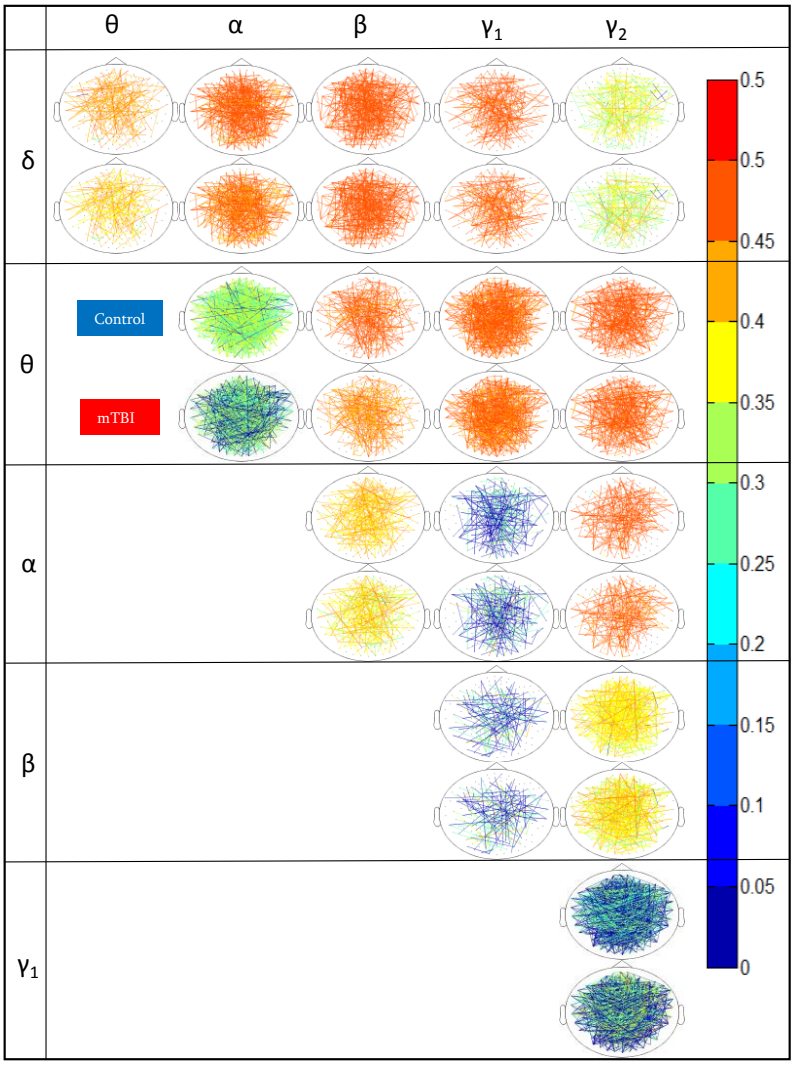

Figure S.6. Topography of the mean CFC connections according to the Laplacian score as feature selection algorithm for each frequency band and group.

Table S6. Classification performance of the vectorization approach (averaged across 10 folds of cross-validation) with k-NN classifier and as input the weights of the FCGs of the two groups based on Laplacian Scores.

Frequency band	θ			α			β			γ1			γ2		
	Accuracy (%)	Sensitivity (%)	Specificity (%)												
δ	38.96±0.83	2.34±1.335	100±0	56.73±1.41	30.76±2.30	100±0	83.58±1.294	73.72±2.07	100±0	53.38±1.64	25.4±2.629	100±0	38.63±0.78	1.8±1.255	100±0
θ				37.5±0	0±0	100±0	73.68±0.63	57.88±1.01	100±0	37.5±0	0±0	100±0	37.5±0	0±0	100±0
α							37.64±0.39	0.22±0.62	100±0	37.5±0	0±0	100±0	39.08±0.93	2.52±1.49	100±0
β										37.61±0.47	0.24±0.65	99.9±0.5715	37.5±0	0±0	100±0
γ1													37.5±0	0±0	100±0

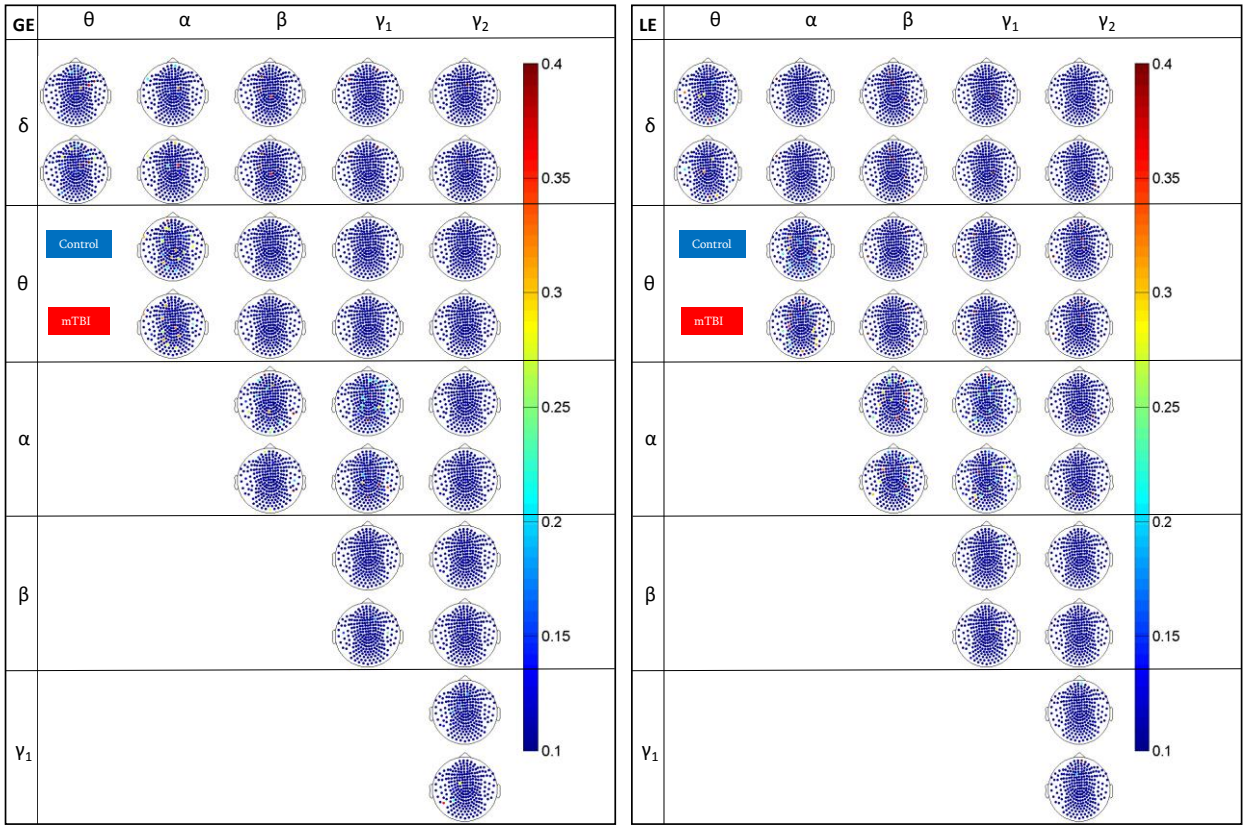

Figure S.7. Topography of the mean CFC Global and Local Efficiency according to the Laplacian score as feature selection algorithm for each frequency band and group.

Table S7. Classification performance of the vectorization approach (averaged across 10 folds of cross-validation) with k-NN classifier and as input global and local efficiency of the full weighted FCGs based on Laplacian Scores.

Frequency band	θ			α			β			γ1			γ2		
	Accuracy (%)	Sensitivity (%)	Specificity (%)												
δ	59.8±4.44	68.54±6.14	45.23±7.25	55.08±4.76	67.36±6.46	34.6±7.69	61.25±4.24	70.64±5.76	45.6±7.77	64.99±4.52	63.42±5.32	67.6±7.71	61.01±4.18	65.32±6.11	53.83±7.5
θ				59.38±3.18	62.56±3.85	54.07±5.66	64.46±4.48	74.44±6.08	47.83±7.57	53.49±4.54	67.38±5.72	30.33±7.75	57.13±4.34	56.56±5.58	58.07±7.11
α							58.1±4.35	78.88±6.05	23.47±8.49	60.35±4.59	60.4±5.66	60.27±7.79	68.33±4.35	80.2±5.57	48.53±6.2
β										61.6±3.86	59.22±5.21	65.57±6.03	67.81±4.11	63.36±5.92	75.23±7.39
γ1													61.14±4.13	71.54±5.05	43.8±6.8

8. Details about subject demographics

Table S8. Subject demographics for the current mTBI group.

Subject	Age at injury	Gender	Auto Pedestrian - frontal	Auto Pedestrian - frontal Type	Auto Pedestrian - frontal _Location
1	21.7	M	Auto Pedestrian	Laceration - no sutures	Head
2	42.0	M	Motor Vehicle	Abrasion	Head
3	22.1	M	Motor Vehicle	Tenderness	Head
4	43.1	M	Motor Vehicle	Tenderness	Head
5	34.6	M	Fall Raised Surface	Abrasion	Head
6	42.3	F	Assault	Bruising	Head
7	20.3	M	Motor Vehicle	Bruising	Head
8	24.0	F	ATV	Laceration - no sutures	Head
9	24.9	M	Sports-related	Laceration - with sutures	Head
10	24.4	F	Motor Vehicle	Bruising	Head/Face
11	43.7	F	Motor Vehicle	Tenderness	Head
12	36.3	M	Blow to Head	Tenderness	Head
13	49.1	M	Motorcycle	Contusion	Head
14	43.3	F	Fall Standing	Laceration - no sutures	Head
15	23.3	F	Fall Standing	Laceration - with sutures	Head
16	33.4	M	Fall Raised Surface	Laceration - no sutures	Head
17	27.3	M	Auto Pedestrian	Tenderness	Head/Face
18	49.8	F	Fall Moving Object	Laceration - with sutures	Head
19	25.3	M	Fall	Abrasion	Head
20	27.7	M	Fall Moving Object	Abrasion	Head
21	20.5	M	Motor Vehicle	Bruising	Head
22	27.0	F	Auto Pedestrian	Bruising	Head
23	22.6	F	Motor Vehicle	Contusion	Head
24	34.8	M	Assault	Contusion	Head
25	20.3	M	Sports-related	Contusion	Head/Face
26	43.8	F	Fall Standing	Contusion	Head
27	28.8	F	Motor Vehicle	Contusion	Head
28	27.8	M	Assault	Contusion	Head
29	24.7	F	Assault	Contusion	Head
30	22.8	F			

References

Bassett, D.S., Meyer-Lindenberg, A., Achard, S., Duke, T., Bullmore, E.T., 2006. Adaptive reconfiguration of fractal small-world human brain functional networks. Proc Natl Acad Sci USA 103, 19518–19523.

Bertoni, A., Folgieri, R., Valentini, G., 2005. Bio-molecular cancer prediction with random subspace ensembles of support vector machines, Neurocomputing 63, 535– 539.

Dietterich, T.G. Ensemble methods in machine learning. In: Proceedings of Multiple Classifier.

Dimitriadis, S.I., Kanatsouli, K., Laskaris, N.A., Tsirka, V., Vourkas, M., Micheloyannis, S., 2012b. Surface EEG shows that Functional Segregation via Phase Coupling contributes to the neural Substrate of Mental Calculations. Brain and Cognition, 80(1), 45–52.

Dimitriadis, S.I., Laskaris, N.A., Del Rio-Portilla, Y., Koudounis, G.C., 2009. Characterizing dynamic functional connectivity across sleep stages from EEG. Brain Topography, 22, 119-133.

Dimitriadis, S.I., Laskaris, N.A., Tsirka, V., Vourkas, M., Micheloyannis, S., 2010b. What does delta band tell us about cognitive Processes: a mental calculation study? Neuroscience Letters 483 (1), 11-15.

Dimitriadis, S.I., Laskaris, N.A., Tsirka, V., Vourkas, M., Micheloyannis, S. 2012a. An EEG study of brain connectivity dynamics at the resting state. Nonlinear Dynamics, Psychology and Life Sciences 16(1), 5-22.

He X, Cai D, Niyogi P. Laplacian score for feature selection. In Advances in Neural Information Processing Systems 18 Weiss, Scholkopf, Platt (editors). MIT Press, Cambridge, MA, 2005.

Ho, T.K., 1998. The random subspace method for constructing decision forests. IEEE Trans. on Pattern Analysis and Machine Intelligence, 20 (8), 832–844.

Huang, D., Yang, B., Tan, B., Rautiainen, M., Zhang, P., Hu, J., Shabanov, N.V., Linder, S., Knyazikhin, Y., Myneni, R.B., 2006. The importance of measurement errors for deriving accurate reference leaf area index maps for validation of moderate-resolution satellite LAI products. IEEE Transactions on Geoscience and Remote Sensing.

Kolchinsky, A., Van Den Heuvel, M.P., Griffa, A., Hagmann, P., Rocha Luis, M., Sporns O., Goni, J., 2014. Multi-scale Integration and Predictability in Resting State Brain Activity, Front Neuroinf 8, 66.

Kuncheva, L.I., Rodriguez, J.J., Plumpton, C.O., Linden, D.E., Johnston, S.J., 2010. Random subspace ensembles for FMRI classification, IEEE Transaction on Medical Imaging, 29(2), 531–542.

Laskaris, N.A., Tarnanas, I., Tsolaki, M.N., Vlaikidis, N., and Karlovasitou, A.K.(2013).Improved detection of amnestic MCI by means of discriminative vector quantization of single-trial cognitive ERP responses. J Neurosci Methods. 30;212(2),344-354.

Leuchter, A.F., Cook, I.A., Newton, T.F., Dunkin, J., Walter, D.O., Rosenberg-Thompson, S., Lachenbruch, P.A, and Weiner, H., 1993. Regional differences in brain electrical activity in dementia: use of spectral power and ratio measures Electroencephalogr. Clin. Neurophysiol. 87 385–93.

Meilă, M., 2007. Comparing clusterings—an information based distance. J. of Multivar. Anal. 98(5), 873-895.

Rodriguez G, Copello F, Vitali P, Perego G and Nobili F 1999 EEG spectral profile to stage Alzheimer's disease Clin.Neurophysiol. 110, 1831–7.

Scheeringa, R., Bastiaansen, M.C.M., Petersson, K.M., Oostenveld, R. , Norris, D.G., Hagoort., P., 2008. Frontal theta EEG activity correlates negatively with the default mode network in resting state. Int. J. Psychophysiol., 67, 242–251.

Skurichina, M., 2002. Bagging, boosting and the random subspace method for linear classifiers. Pattern Analysis and Applications 5(2), 121–135.